Chapter 2
Background

2.1 LED Efficiency

It is well-known that the performance of a LED is governed by the wall-plug efficiency defined as the ratio of total optical output power from emitter to the electrical input power. It indicates how efficiently the electrical power can be converted into optical power and mathematically expressed as the product of four factors, electrical efficiency, injection efficiency, internal quantum efficiency, and light extraction efficiency.

$$\eta_{\text{wall}} = \eta_{\text{ele}} \cdot \eta_{\text{EQE}} = \eta_{\text{ele}} \cdot \eta_{\text{inj}} \cdot \eta_{\text{int}} \cdot \eta_{\text{extraction}} \tag{2.1}$$

The electrical efficiency is primarily limited by ohmic losses and driver losses and shows how the energy can be acquired from the power source to drive an operating LED. The product of remaining parts is regarded as the external quantum efficiency (EQE) which indicates the portion of photons emitted from the devices injected carrier.

2.1.1 Injection Efficiency

Prior to electron-hole recombination, an injection of electron-hole pair into the active layer are necessitated. The injection efficiency is defined as the proportion of injected electrons being able to reach the active region. The injection efficiency can be expressed as:

$$\eta_{\text{inj}} = \frac{J_p}{J_p + J_n + J_s} \tag{2.2}$$

K.H. Li, *Nanostructuring for Nitride Light-Emitting Diodes and Optical Cavities*, Springer Theses, DOI 10.1007/978-3-662-48609-2_2

where J_p is the minority carrier hole diffusion current, J_n is the minority carrier electron diffusion current, and J_s is the space charge recombination current in p-n junction.

2.1.2 Internal Quantum Efficiency

During radiative recombination, an electron from the conduction band directly combines with a hole in the valence band to generate a photon. However, the non-radiative recombination indeed competes with radiative recombination under practical conditions. Such unwanted processes occur via the Auger processes or the defect levels to produce heat or phonons [1]. Internal quantum efficiency (IQE) is the fraction of electron–hole pairs in the active region that can recombine radiatively to produce photons.

$$\eta_{\text{int}} = \frac{P_{\text{int}}/(h\nu)}{I/e} \tag{2.3}$$

where P is the optical power emitted from the active region.

2.1.3 Light Extraction Efficiency

In an ideal scenario, all photons generated at the active region are expected to escape from the LED and enter into free space, achieving unity extraction efficiency. However, in real situation, emitted light may be partially reabsorbed by the LED substrates, active layer, semi-transparent current spreading film, metallic contacts, bonding wires, etc. The light extraction efficiency (LEE) is typically defined as the portion of light generated in the active region that can emit into free space

$$\eta_{\text{ext}} = \frac{P/(h\nu)}{P_{\text{int}}/(h\upsilon)} \tag{2.4}$$

where P is the optical power emitted from the active region into free space.

2.2 Strategies for Light Extraction

The growing demand for blue light LEDs has also prompted for devices with maximal external quantum efficiency (EQE), which is determined by both internal quantum efficiency (IQE) and light extraction efficiency (LEE). With the rapid and

massive improvements of growth techniques, epitaxial structures and crystal quality, the IQE has been greatly enhanced to more than 80 % [2]. However, the extremely low extraction efficiency (<10 %) is still one of the major bottlenecks restricting the performance of LEDs [3], attributed to absorption of substrate, current spreading layer, ohmic contacts and bonding wire, as well as the main challenge of total internal reflection, thus implying that there is still plenty of room for improving the LEE. In the following parts, the influence of total internal reflection is discussed. Numerous approaches aiming to extract optically guided light from devices and suppress total internal reflection are highlighted, including surface roughening, microLEDs, geometrical shaping, and photonic crystal. These methods rely on the formation of nonparallel surfaces to minimize reflections and reduce reabsorption loss, albeit at different dimensional scales.

2.2.1 Total Internal Reflection

Owing to high refractive index contrast at semiconductor/air interface, majority of photons emitted from the active region are remained trapped. The light trapping phenomenon is known as total internal reflection (TIR), strictly limiting the light extraction efficiency of LED (Fig. 2.1). According to Snell's law, TIR occurs when light rays strike on the flat-top semiconductor/air interface with incident angle greater than critical angle

$$\theta_c = \sin^{-1}\left(\frac{n_{\text{air}}}{n_{\text{sc}}}\right) \tag{2.5}$$

where n_{air} *and* n_{sc} are the refractive indexes of air and semiconductor. Photons outside of the escape angle are likely to be reabsorbed after multiple reflections. In particular, the refractive index is about 2.45 for III-nitride semiconductor and the light extraction angle (escape angle or escape cone) is about 23.5°. TIR resulting from the narrow escape cone prevents the photons from escaping from the semiconductor. Moreover, the light extraction efficiency of the top emission surface can be roughly estimated as

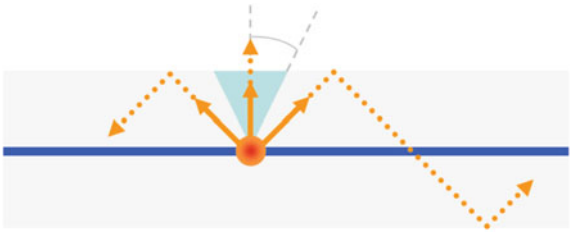

Fig. 2.1 Depicts how the emitted light remains trapped within the device

$$\eta_{\text{ext}} = \int_0^{\theta_c} T_f(\theta)\alpha(\theta, d)\sin\theta d\theta \tag{2.6}$$

where $T_f(\theta)$ is the Fresnel transmission coefficient function and $\alpha(\theta,d)$ is the absorption coefficient function. The flat-top emission surface of the conventional LEDs is found to be as low as 4 % [4] while the overall extraction efficiency is strictly limited to around 12 %.

2.2.2 Surface Roughing

A popular, cost effective and practical approach is to roughen the surface of LED chip via natural chemical etching. Common roughening techniques, including photo-electrochemical chemical etching and wet etching, are capable of developing high-density randomly oriented miniature facets/features on the LED surface [5–8]. The processed surface can randomize the path of trapping and significantly increase the probability for light striking the boundary at an angle close to normal. Surface roughing technique can possibly produce about a factor of enhancement in the light output power and effectively scatter the trapped light outside the LED devices (Fig. 2.2).

2.2.3 MicroLEDs

When emitted, light incidents upon the boundary at angle an greater than critical angle; it suffers total internal reflection and become laterally guided modes, which

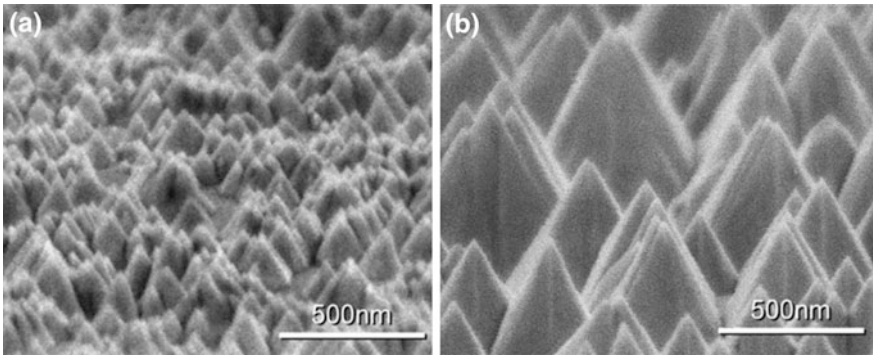

Fig. 2.2 Roughened surface of GaN surface etched by PEC Method. Reprinted from Ref. [5] with permission from AIP Publishing LLC

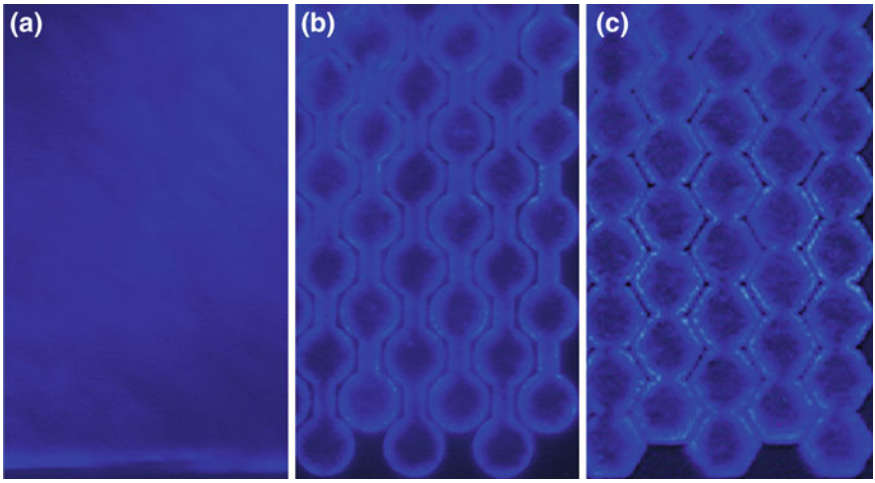

Fig. 2.3 Optical microphotographs showing emission regions of the **a** large-area, **b** microdisk, and **c** microhexagon LEDs. Reprinted from Ref. [9] with permission from AIP Publishing LLC

can either be reabsorbed or escaped from the edges of LED. To increase the changes for light to be extracted into free space before reabsorption, microLEDs provide additional photon escape pathways through the peripheries of microstructures [9–11]. The interconnected microstructures are generally formed by dry etching process so as to remove the material between the microelements, thus significantly increasing the exposed sidewalls [12]. The enhancement in light extraction is attributed to the increased surface area especially the etched sidewall and the CCD images shown in Fig. 2.3, clearly indicate that higher brightness is observed along the edges of microstructures.

2.2.4 Geometrical Shaping

For a conventional LED with cubical geometry, a light ray reflected from one face is likely to hit another parallel facet and bounce around inside the LED chip until it is reabsorbed. One way to overcome this problem is to change the shape of the LED die by creating beveled sidewalls such that the facet pairs are no longer parallel and possibly alter its propagation direction of reflected light [13, 14]. C.C. Kao et al. demonstrated the light output power of a nitride-based LED with 22° undercut sidewall LED was enhanced by 70 % [15]. Moreover, Wang et al. reported various polygonal LEDs shaped with laser micromachining (Fig. 2.4) and proved that LEDs with polygonal geometries increases the light extraction compared to conventional rectangle LEDs [16].

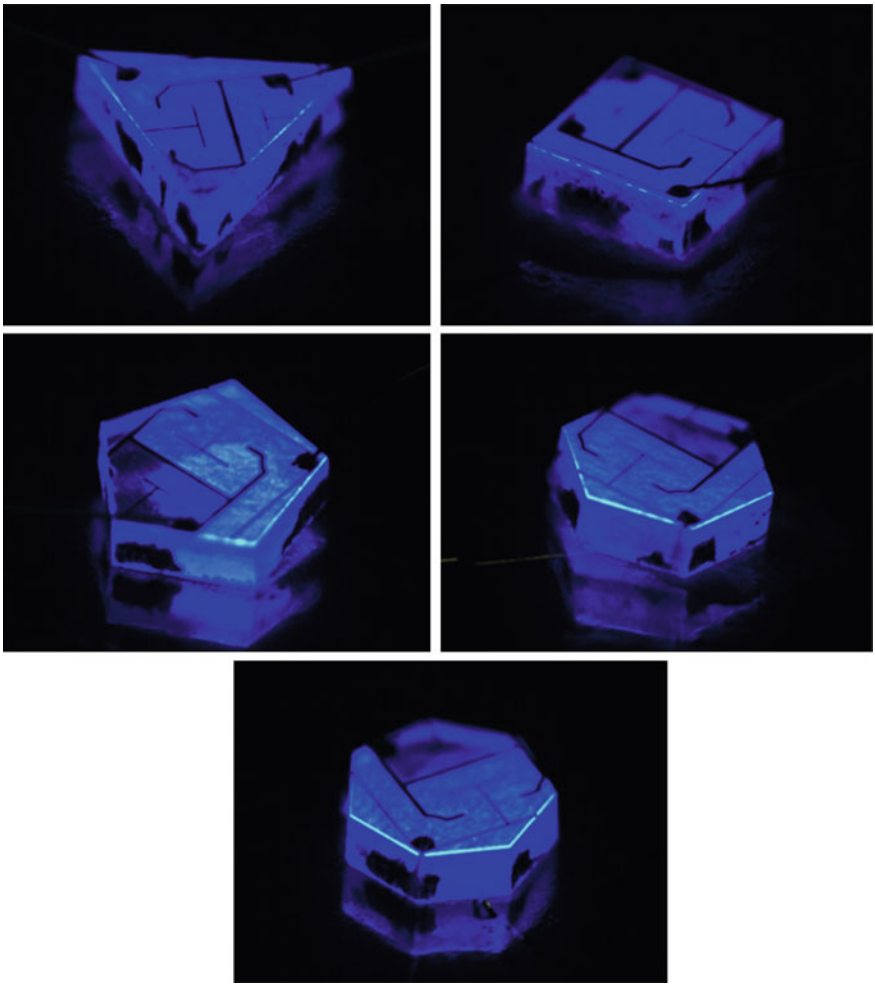

Fig. 2.4 Optical microscopy images of polygonal LED chips. Reprinted from Ref. [16] with permission from AIP Publishing LLC

2.2.5 Photonic Crystal

Photonic crystals (PhCs) [17, 18], with unique capabilities of being able to control and manipulate the propagation of light, have been widely adopted in diverse optoelectronic and photonic applications, including laser resonant cavities [19], high-speed optical fiber transmission [20], and polarization filtering [21]. The incorporation of 2-D PhCs onto the surfaces of nitride-based LEDs enable strong interaction of the guided modes and has also been demonstrated to effectively promote light extraction efficiency [22, 23]. Such ordered periodic nanostructures (Fig. 2.5),

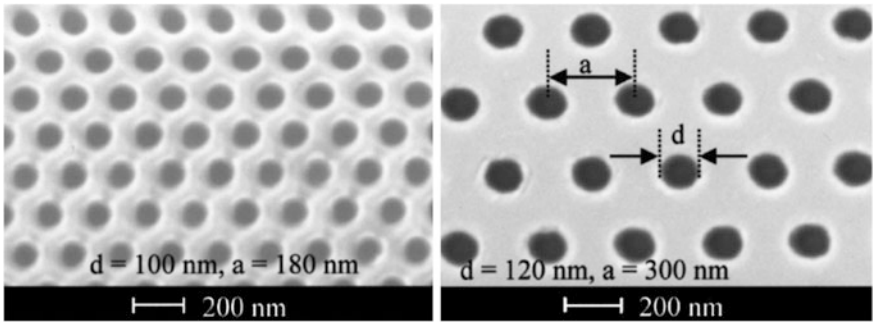

Fig. 2.5 Hexagonal air-hole array patterned by electron-beam lithography (*right*). Reprinted from Ref. [18] with permission from AIP Publishing LLC

with the ability of manipulating spontaneous emission, can be extremely useful for extracting guided modes to air, thus enlarging the escape cone.

The light extraction behaviors of 2-D PhC can be explained by the dispersion diagrams showing normalized frequency versus in-plane wave vector. As illustrated in Fig. 2.6, the green solid line in the band structure, namely the light line, represents a dividing line between guided and leaky modes. With the presence of PhC, band folding will occur at the Brillouin zone edges and guided modes are folded above the air light line, meaning that the guided modes can radiate out form the device. The radiative modes located at the region above the light line corresponds to leaky modes in which the optical mode leaks energy into the surrounding air as it propagates down the waveguide. For the frequency bands that are below the light line, they are the guided modes and do not leak energy as they propagate. Therefore, the light extraction enhancement originates from the coupling of leaky modes above the light line of the band structure. In addition, PhC can also act as

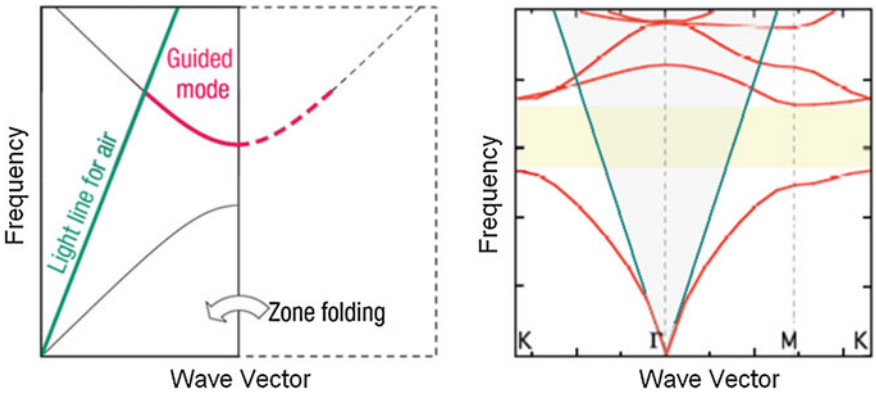

Fig. 2.6 Band diagram illustrating the band folding effect (*left*) and band structure of well-designed PhC (*right*)

2-D diffraction gratings in slabs to extract guided modes to the air and to redirect the emission directions.

With a well-defined periodic arrangement and with sufficiently large refractive index contrast between GaN and ambient, a photonic bandgap (PBG) may be established, which forbids the propagation of light within a specific range of frequencies dependent on the dimension and pitch of the array, as illustrated in Fig. 2.6. The PBG can thus be exploited for suppressing lateral wave-guiding and possibly redirect a significant proportion of trapped photons for extraction, overcoming one of the major limitations of nitride LEDs.

2.3 Lasing Mechanisms

Generally, an optical cavity or resonator, which comprises of two or more mirrors, is capable of confining and storing light at certain resonance frequencies such that a standing wave is established within the cavity. Various optical resonator configurations are depicted in Fig. 2.7. The most common one, so called Fabry–Pérot (F-B) resonator [24, 25], comprises two parallel planar mirrors and forces the light to bounce back and forth within them. Those mirrors can be formed by periodic dielectric mirror such as distributed Bragg reflector (DBR) to confine light with desired frequency in a particular direction. The resonant mode occurs when an integral multiple of half-wavelengths fit into the cavity spacing of length.

Whispering-gallery (WG) mode [26, 27] is mostly constructed within the circular, hemispherical, or even elliptical cavities. When light is propagating around the edge of cavity, it will be totally reflected at boundary of resonator and confined a closed circular path. Thereby, the confined ray propagates around the inside rim of a resonator with its incident angle greater than the critical angle. In order to obtain constructive interference, the propagation path per cycle, which is approximately equal to the circumference of resonator, should be an integer multiple of wavelength of light.

Two-dimensional (2-D) photonic crystals (PhCs) with defects are also used to make microcavities [28, 29]. The periodic dielectric structure exhibits photonic bandgaps which are able to suppress the propagation of light with the bandgap frequency ranges. A defect in the 2-D periodic PhCs can be designed as a missing element in an air-hole array. For the wavelengths overlapping with the PBG, the periodic structure surrounding the defect acts as the reflector, so that light is trapped within the defect. The defect is then regarded as a microcavity resonator and possibly provides extremely small mode volume and high Q-factor exceeding 10^5, but the main challenge for such cavities are the difficulty for its precise design and fabrication.

Those optical resonators are the common light-confinement mechanisms adopted for semiconductor lasers. The optical path lengths of such cavities, dependent on the vertical heights of F–P cavities, or lateral dimensions of WG circular cavities and photonic bandgap (PBG) structures, are crucial factors determining the lasing

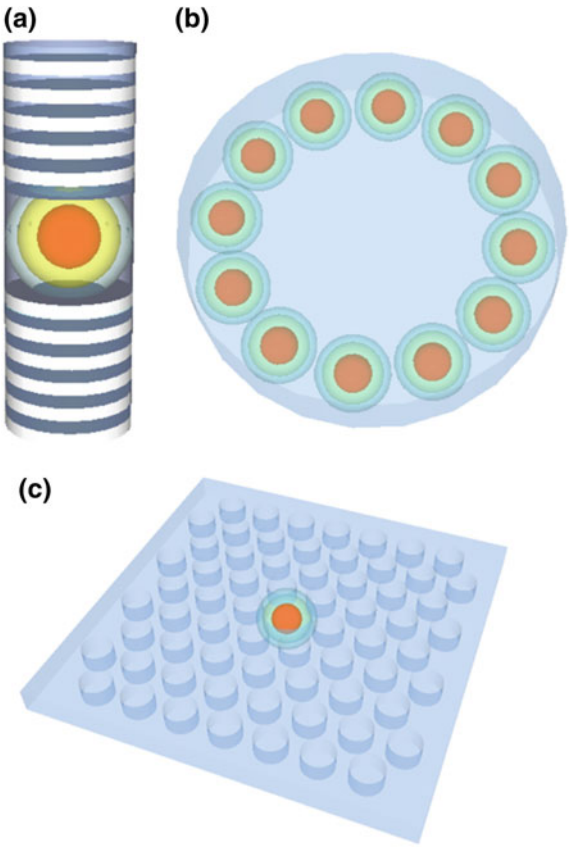

Fig. 2.7 Schematic diagrams depicting three common light-confinement mechanisms: **a** Fabry–Pérot, **b** whispering-gallery, and **c** 2-D photonic crystal defect cavities

characteristics. To confine propagating photons in controllable and predictable manner, these optical cavities are usually designed to be of the order of the wavelength or even at subwavelength scales.

2.4 Quality Factor and Loss of a Resonant Cavity

The quality factor (Q factor) is a key figure of merit for resonator and defined as the fraction of the energy stored in a cavity to the energy dissipated per cycle. For example, high value of Q factor corresponds to a low rate of energy loss relative to the stored energy of a resonator. The value of Q factor can be simply calculated by measuring the spectrum of the resonant mode

$$Q = \frac{\lambda}{\Delta\lambda} \tag{2.7}$$

where λ is the resonant wavelength, and $\Delta\lambda$ is the full-width-at-half-maximum (FWHM) of the resonant peak. An ideal cavity/resonator offers an infinite value of Q factor, meaning that there is no energy dissipated per cycle. In practical applications, a resonant cavity always experiences the energy losses comprising of material absorption loss, scattering loss, radiation loss, and coupling loss. The sum of the first three loss mechanisms is referred to as the intrinsic loss of a resonator while the overall Q factor can be determined by the individual loss terms:

$$\frac{1}{Q} = \frac{1}{Q_{\text{abs}}} + \frac{1}{Q_S} + \frac{1}{Q_{\text{rad}}} + \frac{1}{Q_C} \tag{2.8}$$

where Q_{abs} corresponds to the light absorption of the material; Q_S is related to the scattering loss due to surface inhomogeneities and contaminants; Q_{rad} is the radiation loss originated from the escape of light energy through a curvature surface; and Q_C is the loss induced by a waveguide coupling. Scattering loss can be reduced by improving the fabrication process to minimize the resonator surface roughness. Radiation loss strongly depends on the size of a resonator and can be reduced by increasing the cavity size. It is also worth noting that when the resonator size is larger than some certain dimension, the radiation loss will become negligible compared to other loss mechanisms.

2.5 Nanosphere Lithography

As the characteristic length scales of PhCs structures and the dimension of resonators are of the order of the wavelength, nanopatterning techniques are involved during fabrication of short-wavelength optoelectronic devices, often increasing manufacturing costs. Unlike conventional AlInGaP emitters which can be processed by standard microlithographic techniques, the blue/UV PhC and cavities require further dimensional shrinkage in order to fulfill constraints associated with short-wavelength light interaction, so that traditional optical patterning techniques are no longer able to offer the required resolutions due to the diffraction limit. While direct-write techniques such as electron-beam lithography (EBL) [18, 30] and focused ion beam (FIB) milling [31, 32] are capable of producing arbitrary 2-D feature accurately down to the nanometer scale, they also each have their own drawbacks. The nanofabrication methods are summarized in Table 2.1. High equipment cost and time-consuming point-by-point processing and thus low throughput make large-volume manufacturing impractical. To overcome such limitations, a high-throughput yet low-cost approach is introduced that is particularly suitable for the processing of hard nitride semiconductors: nanosphere lithography (NSL).

Table 2.1 Comparison of nanofabrication methods

	EBL	FIB	NSL
Etch selectivity	Low	N/A	High
Equipment cost	High	High	Low
Preparation time	Long	Long	Short

2.5.1 Overview

Nanosphere lithography (NSL) [33] is an inexpensive and ultra-efficient nanopatterning technique with attractive abilities of producing well-ordered periodic arrays over large areas with minimal processing time. With wide ranges of commercially-available sphere dimensions from hundreds of micrometer down to tens of nanometers, the spheres can self-assemble into mono- and multi-layers of periodically ordered array (Fig. 2.8). Nanospheres have previously found uses in technologies such as catalysis, biochemical devices, cell cultures, surface-enhanced Raman spectroscopy, and sensing application. In the field of optoelectronics, ordered periodic structures based on nanospheres may be used as PhCs to manipulate the flow of light; in particular, 3-D PhCs [34–36] which can interact with light in both the vertical and lateral directions. In this chapter, we shall mainly focus on lithographic processes for generating 2-D monolayers of silica spheres which serve as high etch selectivity masks for GaN materials during dry etch, with the target of producing various 2-D regular nanostructure arrays on the surface of the wafer. We shall first discuss the fundamental steps in the formation of self-assembled ordered monolayer in hexagonal-close-packed (HCP) arrangement for pattern transfer.

2.5.2 Process Development

The formation of an ordered HCP monolayer over large areas on a substrate is commonly achieved via one of the three coating strategies including vertical

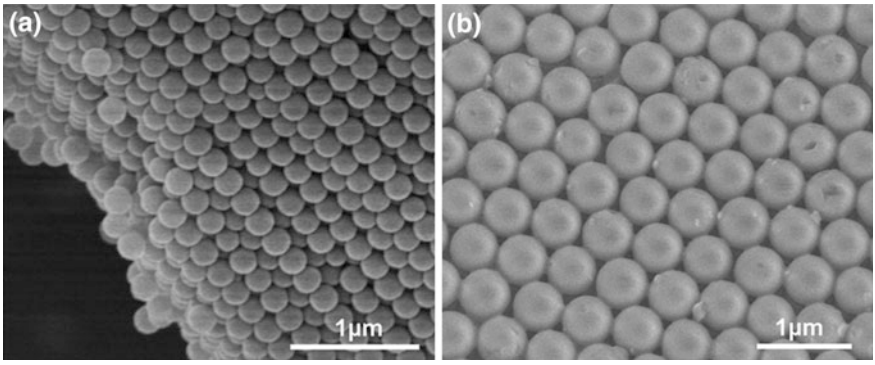

Fig. 2.8 FE-SEM images of **a** multilayers and **b** monolayer of spheres

deposition, dip-coating, and spin-coating, as illustrated in schematic diagrams in Fig. 2.9. The successes of these strategies are dependent on various factors determining quality of the coated monolayer. If the processing conditions are suboptimal, the spheres will simply aggregate to form undesirable clusters, or spread out loosely without any particular order. Due to the low-withdrawal speed in dip-coating and slow evaporation rate in vertical deposition, long processing time (of the order of hours) may be required to establish a monolayer over centimeter-scale areas. Moreover, it is often difficult to maintain precise control of the ambient conditions, such as temperature, humidity, and pressure which strongly affect the evaporation rate. On the other hand, the spin-coating method, which is mainly governed by rotation speed, concentration, size of spheres, and wettability of substrate, is a more reliable method with distinct advantages of higher throughput and better reproducibility. The areas of close-packed monolayer are typically of the order $\sim cm^2$, while the equipment cost of spin-coating technique is low. When these parameters are fine-tuned, monolayer arrays of close-packed nanospheres over centimeters can be obtained within a matter of minutes.

Uniform silica nanospheres are initially diluted in deionized water to produce the optimal volume concentration of ~ 2 %. The diluted colloidal suspension is then mixed with sodium dodecyl sulfate at a volume ratio of 10:1. Introduction of a surfactant lowers the surface tension of the colloidal suspension and thus facilitates the spreading of nanosphere to prevent particle agglomeration or aggregation. The well-mixed colloidal suspension is then carefully dispensed onto the sample surface by mechanical micropipetting or other means. Optimized rotational speed is necessary to balance the centrifugal force with the solvent capillary force. During spin-coating, the excess suspension is gradually flung off and spheres spread laterally, self-assembling into a monolayer of hexagonal-close-packed array across the sample. The coated spheres then act as a lithographic mask and the pillar pattern is transferred to the wafer by inductive-coupled plasma (ICP) etching. The etched

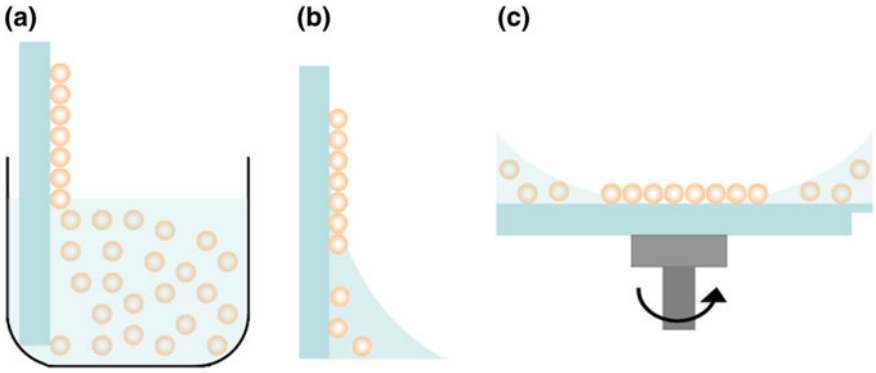

Fig. 2.9 Schematic diagrams showing various nanosphere coating procedures, including **a** vertical deposition, **b** dip-coating, and **c** spin-coating

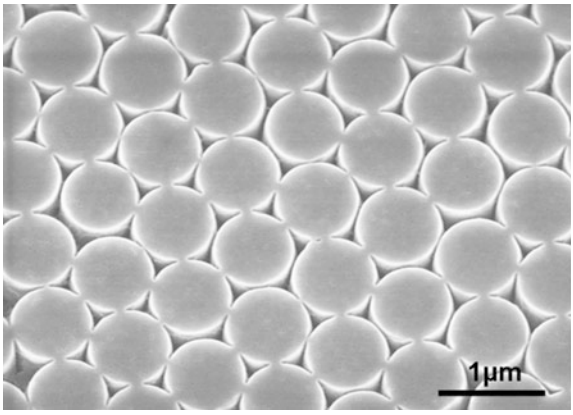

Fig. 2.10 FE-SEM images of an HCP nanopillar array patterned by NSL

sample is finally immersed in deionized water under sonication to remove the spheres, leaving behind a nanopillar array. The resultant HCP nanopillar array after etching is shown in Fig. 2.10.

References

1. Heikkila O, Oksanen J, Tulkki J (2010) The challenge of unity wall plug efficiency: the effects of internal heating on the efficiency of light emitting diodes. J Appl Phys 107(3). Artn 033105. doi: 10.1063/1.3285431
2. Akasaka T, Gotoh H, Saito T, Makimoto T (2004) High luminescent efficiency of InGaN multiple quantum wells grown on InGaN underlying layers. Appl Phys Lett 85(15):3089−3091. doi: 10.1063/1.1804607
3. David A, Fujii T, Sharma R, McGroddy K, Nakamura S, DenBaars SP, Hu EL, Weisbuch C, Benisty H (2006) Photonic-crystal GaN light-emitting diodes with tailored guided modes distribution. Appl Phys Lett 88(6). Artn 061124. doi:10.1063/1.2171475
4. Lester SD, Ponce FA, Craford MG, Steigerwald DA (1995) High dislocation densities in high-efficiency gan-based light-emitting-diodes. Appl Phys Lett 66(10):1249−1251. doi: 10.1063/1.113252
5. Fujii T, Gao Y, Sharma R, Hu EL, DenBaars SP, Nakamura S (2004) Increase in the extraction efficiency of GaN-based light-emitting diodes via surface roughening. Appl Phys Lett 84(6):855−857. doi: 10.1063/1.1645992
6. Minsky MS, White M, Hu EL (1996) Room-temperature photoenhanced wet etching of GaN. Appl Phys Lett 68(11):1531–1533. doi:10.1063/1.115689
7. Gao Y, Fujii T, Sharma R, Fujito K, Denbaars SP, Nakamura S, Hu EL (2004) Roughening hexagonal surface morphology on laser lift-off (LLO) N-face GaN with simple photo-enhanced chemical wet etching. Jpn J Appl Phys 243(5A):L637-L639. doi:10.1143/Jjap.43.L637
8. Yang CC, Horng RH, Lee CE, Lin WY, Pan KF, Su YY, Wuul DS (2005) Improvement in extraction efficiency of GaN-based light-emitting diodes with textured surface layer by natural lithography. Jpn J Appl Phys 144(4B):2525–2527. doi:10.1143/Jjap.44.2525
9. Li ZL, Li KH, Choi HW (2010) Mechanism of optical degradation in microstructured InGaN light-emitting diodes. J Appl Phys 108(11). Artn 114511. doi:10.1063/1.3517829

10. Jin SX, Li J, Lin JY, Jiang HX (2000) InGaN/GaN quantum well interconnected microdisk light emitting diodes. Appl Phys Lett 77(20):3236–3238. Pii [S0003-6951(00)04546-0]. doi:10.1063/1.1326479
11. Choi HW, Dawson MD, Edwards PR, Martin RW (2003) High extraction efficiency InGaN micro-ring light-emitting diodes. Appl Phys Lett 83(22):4483–4485. doi:10.1063/1.1630352
12. Choi HW, Chua SJ (2006) Honeycomb GaN micro-light-emitting diodes. J Vac Sci Technol B 24(2):800–802. doi:10.1116/1.2184324
13. Lee YC, Lee CE, Kuo HC, Lu TC, Wang SC (2008) Enhancing the light extraction of (AlxGa1-x)(0.5) In0.5P-based light-emitting diode fabricated via geometric sapphire shaping. IEEE Photonic Tech L 20(5-8):369-371. doi:10.1109/Lpt.2008.916905
14. Lee CE, Lee YC, Kuo HC, Tsai MR, Lu TC, Cwang S (2008) High brightness GaN-based flip-chip light-emitting diodes by adopting geometric sapphire shaping structure. Semicond Sci Tech 23(2). Artn 025015. doi:10.1088/0268-1242/23/2/025015
15. Kao CC, Kuo HC, Huang HW, Chu JT, Peng YC, Hsieh YL, Luo CY, Wang SC, Yu CC, Lin CF (2005) Light-output enhancement in a nitride-based light-emitting diode with 22 degrees undercut sidewalls. IEEE Photonic Tech L 17(1):19–21. doi:10.1109/Lpt.2004.837480
16. Wang XH, Lai PT, Choi HW (2010) The contribution of sidewall light extraction to efficiencies of polygonal light-emitting diodes shaped with laser micromachining. J Appl Phys 108(2). Artn 023110. doi:10.1063/1.3456445
17. Kim SH, Lee KD, Kim JY, Kwon MK, Park SJ (2007) Fabrication of photonic crystal structures on light emitting diodes by nanoimprint lithography. Nanotechnology 18(5). Artn 055306. doi:10.1088/0957-4484/18/5/055306
18. Oder TN, Shakya J, Lin JY, Jiang HX (2003) III-nitride photonic crystals. Appl Phys Lett 83(6):1231–1233. doi:10.1063/1.1600839
19. Matsubara H, Yoshimoto S, Saito H, Yue JL, Tanaka Y, Noda S (2008) GaN photonic-crystal surface-emitting laser at blue-violet wavelengths. Science 319(5862):445–447. doi:10.1126/science.1150413
20. Knight JC (2003) Photonic crystal fibres. Nature 424 (6950):847–851. doi:10.1038/Nature01940
21. Lai CF, Chi JY, Yen HH, Kuo HC, Chao CH, Hsueh HT, Wang JFT, Huang CY, Yeh WY (2008) Polarized light emission from photonic crystal light-emitting diodes. Appl Phys Lett 92(24). Artn 243118. doi:10.1063/1.2938885
22. Wierer JJ, Krames MR, Epler JE, Gardner NF, Craford MG, Wendt JR, Simmons JA, Sigalas MM (2004) InGaN/GaN quantum-well heterostructure light-emitting diodes employing photonic crystal structures. Appl Phys Lett 84(19):3885–3887. doi:10.1063/1.1738934
23. Kim DH, Cho CO, Roh YG, Jeon H, Park YS, Cho J, Im JS, Sone C, Park Y, Choi WJ, Park QH (2005) Enhanced light extraction from GaN-based light-emitting diodes with holographically generated two-dimensional photonic crystal patterns. Appl Phys Lett 87(20). Artn 203508. doi:10.1063/1.2132073
24. Redwing JM, Loeber DAS, Anderson NG, Tischler MA, Flynn JS (1996) An optically pumped GaN-AlGaN vertical cavity surface emitting laser. Appl Phys Lett 69(1):1–3. doi:10.1063/1.118104
25. Someya T, Werner R, Forchel A, Catalano M, Cingolani R, Arakawa Y (1999) Room temperature lasing at blue wavelengths in gallium nitride microcavities. Science 285(5435):1905–1906. doi:10.1126/science.285.5435.1905
26. Tamboli AC, Haberer ED, Sharma R, Lee KH, Nakamura S, Hu EL (2007) Room-temperature continuous-wave lasing in GaN/InGaN microdisks. Nat Photonics 1(1):61–64. doi:10.1038/nphoton.2006.52
27. Mair RA, Zeng KC, Lin JY, Jiang HX, Zhang B, Dai L, Botchkarev A, Kim W, Morkoc H, Khan MA (1998) Optical modes within III-nitride multiple quantum well microdisk cavities. Appl Phys Lett 72(13):1530–1532. doi:10.1063/1.120573

28. Lu TC, Chen SW, Lin LF, Kao TT, Kao CC, Yu P, Kuo HC, Wang SC, Fan SH (2008) GaN-based two-dimensional surface-emitting photonic crystal lasers with AlN/GaN distributed Bragg reflector. Appl Phys Lett 92(1). Artn 011129. doi:10.1063/1.2831716
29. Lai CF, Yu P, Wang TC, Kuo HC, Lu TC, Wang SC, Lee CK (2007) Lasing characteristics of a GaN photonic crystal nanocavity light source. Appl Phys Lett 91(4). Artn 041101. doi:10.1063/1.2759467
30. Oder TN, Kim KH, Lin JY, Jiang HX (2004) III-nitride blue and ultraviolet photonic crystal light emitting diodes. Appl Phys Lett 84(4):466–468. doi:10.1063/1.1644050
31. Motayed A, Davydov AV, Vaudin MD, Levin I, Melngailis J, Mohammad SN (2006) Fabrication of GaN-based nanoscale device structures utilizing focused ion beam induced Pt deposition. J Appl Phys 100(2). Artn 024306. doi:10.1063/1.2215354
32. Lanyon YH, De Marzi G, Watson YE, Quinn AJ, Gleeson JP, Redmond G, Arrigan DWM (2007) Fabrication of nanopore array electrodes by focused ion beam milling. Anal Chem 79 (8):3048–3055. doi:10.1021/Ac061878x
33. Haynes CL, Van Duyne RP (2001) Nanosphere lithography: A versatile nanofabrication tool for studies of size-dependent nanoparticle optics. J Phys Chem B 105(24):5599–5611. doi:10.1021/Jp010657m
34. Ozin GA, Yang SM (2001) The race for the photonic chip: Colloidal crystal assembly in silicon wafers. Adv Funct Mater 11(2):95–104. doi:10.1002/1616-3028(200104)11:2<95::Aid-Adfm95>3.0.Co;2-O
35. Zhang Q, Li KH, Choi HW (2012) Polarized emission from InGaN Light-emitting Diode with Self-assembled opal coating. 2012 12th IEEE conference on nanotechnology (IEEE-Nano)
36. Zhang Q, Li KH, Choi HW (2012) Polarized emission from InGaN light-emitting diodes with self-assembled nanosphere coatings. IEEE Photonic Tech L 24(18):1642–1645. doi:10.1109/Lpt.2012.2211586

http://www.springer.com/978-3-662-48607-8

Nanostructuring for Nitride Light-Emitting Diodes and Optical Cavities

Li, K.H.

2016, XV, 107 p. 101 illus., 15 illus. in color., Hardcover
ISBN: 978-3-662-48607-8